Identifiability Analysis of Non-Integer Antenna Arrays in the Presence of Mixed (Strong and Weak) Signals

Md. Waqeeb T. S. Chowdhury [†], Yimin D. Zhang [†], and Braham Himed [‡]

[†] Department of Electrical and Computer Engineering, Temple University, Philadelphia, PA 19122, USA
[‡] Distributed RF Sensing Branch, Air Force Research Laboratory, WPAFB, OH 45433, USA

***Abstract*—In this paper, we consider the direction-of-arrival (DOA) estimation problem using a non-integer antenna array, and our objective is to examine the effect of sensor placement on the number of array degrees-of-freedom (DOFs) in the presence of a mixture of strong and weak signals. Two scenarios corresponding to off-grid sensor placement are considered: (1) when a single sensor of a uniform linear array (ULA) is in an off-grid position and (2) when the entire ULA is compressed. The smallest signal-subspace eigenvalue corresponding to the weak signals is compared with the rank-revealing QR factorization-based threshold that separates the signal subspace from the noise subspace, providing insights into the numerical rank of the data covariance matrix and serving as a measure of the DOFs of the array. Furthermore, the effect of signal strength on the eigenvalues of the data covariance matrix is studied. The effect of off-grid sensor placement and the variation of the signal strengths on the array DOFs is demonstrated with simulation results.**

Keywords: Degrees-of-freedom, non-integer arrays, weak signals, eigenvalue interlacing property rank analysis, QR factorization.

I. Introduction

Direction finding using sensor arrays is a fundamental problem in array signal processing with many engineering applications, such as radar, sonar, wireless communications, and radio astronomy [1–3]. Conventional uniform linear arrays (ULAs) with a half-wavelength inter-element spacing are designed to spatially sample the signals at the Nyquist sampling rate. The number of degrees-of-freedom (DOFs) of an N-element ULA is limited to $N-1$, making them ineffective in terms of the number of signals that can be resolved for a given number of antennas. To achieve increased sensing capability, sparse linear array structures are developed to provide $\mathcal{O}(N^2)$ DOFs [4–13].

Most of the sparse array structures studied in the literature are thinned from a ULA with sensors placed on a half-wavelength grid. An array is referred to as an integer array when all sensor positions are integer multiples of the half-wavelength, whereas arrays that violate this condition, i.e., some sensors are placed off the half-wavelength grid, are referred to as non-integer arrays [14–16]. The application of non-integer arrays to interference suppression and direction-of-arrival (DOA) estimation was considered in [17, 18]. The Toeplitz property of the covariance matrices for ULAs is not shared by non-integer arrays and an interpolation technique was proposed in [17]. It is found in [18] that optimized non-integer linear arrays provide improved interference cancellation performance. Furthermore, optimized design of non-redundant sparse non-integer linear arrays was studied in [19].

Recently, non-integer arrays are exploited to develop rational arrays in [16, 20], where their performance as well as the conditions for unique identifiability are analyzed. The design of multi-frequency rational sparse arrays, leveraging the extension of the concept of rational sparse arrays with reduced frequency separation, is explored in [21]. The use of rational frequencies provides flexibility in designing multi-frequency and frequency-switching sparse arrays and the resulting virtual rational coprime arrays, as highlighted in previous works [22–25]. However, it becomes crucial to consider spatial correlation and sidelobe issues. In light of this, the study in [26] examines the conditions for unique identifiability and unambiguous source detection. It is worth noting that, although non-integer arrays have been explored for a variety of purposes, there has been limited research into their identifiability. While there are reported results on the impact of sensor placement deviations from a half-wavelength grid on the achievable number of DOFs [27], the full understanding of how the off-grid positioning of sensors affects the achievable DOFs remains incomplete.

In this paper, we investigate such a problem with an emphasis of the presence of mixed (strong and weak) signals as often encountered in radar applications. We provide an analysis of the eigenvalues of the array signal covariance matrix in the presence of weak signals in comparison to the eigenvalues of the covariance matrix when all signals have equal power. The rank-revealing properties of the QR factorization is exploited to define a threshold for the separation between the smallest eigenvalue corresponding to the signal subspace (SS) and the largest eigenvalue corresponding to the noise subspace (NS). The identifiability analysis results are verified using the MUSIC spectrum for different scenarios.

Notations: We use bold lower-case (upper-case) characters to represent vectors (matrices). Specifically, $\mathbf{I}_N$ denotes the $N \times N$ identity matrix, and $\mathbf{0}$ represents a vector or matrix filled with zeros of an appropriate dimension. The symbols

This material is based upon work supported by the Air Force Office of Scientific Research under award number FA9550-23-1-0255. Any opinions, findings, and conclusions or recommendations expressed in this material are those of the authors and do not necessarily reflect the views of the United States Air Force.

$(\cdot)^*$, $(\cdot)^{\mathrm{T}}$, and $(\cdot)^{\mathrm{H}}$ denote complex conjugation, transpose, and Hermitian operations, respectively. $\mathrm{diag}(\cdot)$ constructs a diagonal matrix, and $\mathrm{Tr}(\cdot)$ represents the trace operator. $\mathbb{E}(\cdot)$ denotes the statistical expectation. Additionally, $\jmath = \sqrt{-1}$ denotes the unit imaginary number. $||\mathbf{B}||_2$ denotes the spectral norm of matrix $\mathbf{B}$ and equals the largest singular value of $\mathbf{B}$. Finally, $\mathbb{C}^{M\times N}$ denotes the $M \times N$ complex space.

II. Signal Model

Consider L mutually uncorrelated narrowband signals impinging on an N-element ULA from far field with distinct angles $\boldsymbol{\theta} = [\theta_1, \cdots, \theta_L]^{\mathrm{T}}$, where $L < N$ is assumed. The baseband signal vector observed at the array is given as

$$\mathbf{x}(t) = \sum_{l=1}^{L} \mathbf{a}(\theta_l) s_l(t) + \mathbf{n}(t) = \mathbf{A}\mathbf{s}(t) + \mathbf{n}(t), \tag{1}$$

where

$$\mathbf{a}(\theta) = [e^{-\jmath p_1 \pi \sin(\theta)}, e^{-\jmath p_2 \pi \sin(\theta)}, \ldots, e^{-\jmath p_N \pi \sin(\theta)}]^{\mathrm{T}} \tag{2}$$

is the steering vector of the array corresponding to angle θ, and $\mathbf{A} = [\mathbf{a}(\theta_1), \mathbf{a}(\theta_2), \ldots, \mathbf{a}(\theta_L)] \in \mathbb{C}^{N\times L}$ denotes the manifold matrix of the array. $p_n = n - 1$ represents the position of the nth sensor scaled to the unit inter-element spacing of half-wavelength, $s_l(t)$ denotes the waveform of the lth signal, and the waveforms of the L signals is stacked as a vector $\mathbf{s}(t) = [s_1(t), \cdots, s_L(t)]^{\mathrm{T}}$. In addition, $\mathbf{n}(t) \sim \mathcal{CN}(\mathbf{0}, \sigma_{\mathrm{n}}^2 \mathbf{I}_N)$ represents the zero-mean additive circularly complex white Gaussian noise vector. The covariance matrix of the received data vector $\mathbf{x}(t)$ is expressed as

$$\mathbf{R}_x = \mathbb{E}[\mathbf{x}(t)\mathbf{x}^{\mathrm{H}}(t)] = \mathbf{A}\mathbf{R}_s\mathbf{A}^{\mathrm{H}} + \sigma_{\mathrm{n}}^2 \mathbf{I}_N, \tag{3}$$

where $\mathbf{R}_s = \mathbb{E}[\mathbf{s}(t)\mathbf{s}^{\mathrm{H}}(t)] = \mathrm{diag}\left(\left[\sigma_1^2, \sigma_2^2, \ldots, \sigma_L^2\right]\right)$ is the source covariance matrix.

In practice, the perfect statistics of the covariance matrix are unknown. Instead, we use the sample covariance matrix, which is estimated using K available snapshots as

$$\hat{\mathbf{R}}_x = \frac{1}{K}\sum_{t=1}^{K} \mathbf{x}(t)\mathbf{x}^{\mathrm{H}}(t). \tag{4}$$

Performing an eigen-decomposition of the sample covariance matrix leads to

$$\hat{\mathbf{R}}_x = \sum_{p=1}^{L} \hat{\lambda}_p \hat{\mathbf{u}}_p \hat{\mathbf{u}}_p^{\mathrm{H}} + \sum_{q=L+1}^{N} \hat{\lambda}_q \hat{\mathbf{u}}_q \hat{\mathbf{u}}_q^{\mathrm{H}}, \tag{5}$$

where $\hat{\lambda}_p$ and $\hat{\mathbf{u}}_p$, $p = 1, \ldots, L$, respectively denote the eigenvalues and the corresponding eigenvectors in the SS, whereas $\hat{\lambda}_q$ and $\hat{\mathbf{u}}_q$, $q = L+1, \ldots, N$, are the eigenvalues and the corresponding eigenvectors in the NS.

When the number of available data snapshots approaches infinity, the NS eigenvalues asymptotically approach the noise power σ_n^2. In practice, however, the number of snapshots is limited and the estimated NS eigenvalues are related as $\hat{\lambda}_1 \geq \hat{\lambda}_2 \geq \cdots \geq \hat{\lambda}_L > \hat{\lambda}_{L+1} \geq \cdots \geq \hat{\lambda}_N \approx \sigma_{\mathrm{n}}^2$.

To ascertain the dimension of the signal subspace, we aim to establish a suitable threshold $\hat{\lambda}_{\mathrm{thr}}$ that separates the smallest SS eigenvalue $\hat{\lambda}_L$ and the largest NS eigenvalue $\hat{\lambda}_{L+1}$ such that $\hat{\lambda}_L > \hat{\lambda}_{\mathrm{thr}} > \hat{\lambda}_{L+1}$. This task is not necessarily easy, particularly when the statistics of the received data cannot be accurately estimated and some signals are weak [28]. Furthermore, when one or more sensors are placed along the off-grid positions, the smallest SS eigenvalue will become even closer to the largest NS eigenvalue, making it more challenging to define such a boundary to separate the SS and the NS.

In this paper, we adopt a strategy to define such a threshold by exploiting the rank-revealing properties of the QR factorization [29, 30]. The threshold $\hat{\lambda}_{\mathrm{thr}}$ that separates the SS and the NS can be utilized to determine the numerical rank of the data covariance matrix $\hat{\mathbf{R}}_x$. The numerical rank of the covariance matrix is defined as [27]:

Definition: For a tolerance $\mathcal{O}(\epsilon) > 0$, the numerical rank of $\hat{\mathbf{R}}_x \in \mathbb{C}^{N\times N}$ is the smallest integer $r \leq N$ such that $\lambda_r > \sigma_{\mathrm{n}}^2 + \mathcal{O}(\epsilon)$.

The notion of numerical rank, as explored in [31, 32], combined with the rank-revealing properties of the QR factorization, can be applied to investigate the identifiability of the antenna array in the underlying problem. Consider the case where $\hat{\mathbf{R}}_x$ has a numerical rank of r, and there exists a permutation matrix $\boldsymbol{\Pi} \in \{0,1\}^{N\times N}$ such that the QR factorization of $\hat{\mathbf{R}}_x\boldsymbol{\Pi}$ is given as

$$\hat{\mathbf{R}}_x\boldsymbol{\Pi} = \mathbf{Q}\mathbf{R}, \tag{6}$$

where $\mathbf{Q} \in \mathbb{C}^{N\times N}$ is a unitary matrix, and

$$\mathbf{R} = \begin{bmatrix} \mathbf{R}_{11} & \mathbf{R}_{12} \\ \mathbf{0} & \mathbf{R}_{22} \end{bmatrix} \in \mathbb{C}^{N\times N} \tag{7}$$

is an upper triangular matrix with $\mathbf{R}_{11} \in \mathbb{C}^{L\times L}$ and $\mathbf{R}_{22} \in \mathbb{C}^{(N-L)\times(N-L)}$. In this case, if

$$\lambda_{\min}(\mathbf{R}_{11}) > ||\mathbf{R}_{22}||_2, \tag{8}$$

then Eqn. (6) is said to be a rank-revealing QR factorization of $\hat{\mathbf{R}}_x$ [32]. As the array covariance matrix maintains full rank in the presence of noise, there exists a permutation matrix $\boldsymbol{\Pi}$ such that the diagonal entries of the upper triangular matrix $\mathbf{R}$ are arranged in a decreasing order. Given that the eigenvalues of an upper triangular matrix are the same as its diagonal entries [33], condition (8) is satisfied for any array covariance matrix $\hat{\mathbf{R}}_x$, ensuring the existence of its rank-revealing QR factorization.

Utilizing the interlacing property of eigenvalues [34, 35], it can be demonstrated that $\hat{\lambda}_r(\hat{\mathbf{R}}_x) = \hat{\lambda}_L \geq \lambda_{\min}(\mathbf{R}_{11})$ and $||\mathbf{R}_{22}||_2 \geq \hat{\lambda}_{r+1}(\hat{\mathbf{R}}_x) = \hat{\lambda}_{L+1}$ consistently hold. Therefore, we have

$$\hat{\lambda}_L \geq \lambda_{\min}(\mathbf{R}_{11}) > ||\mathbf{R}_{22}||_2 \geq \hat{\lambda}_{L+1} \approx \sigma_{\mathrm{n}}^2 + \mathcal{O}(\epsilon). \tag{9}$$

From this result, we observe that the spectral norm of $\mathbf{R}_{22}$ can serve as an appropriate threshold value, $\hat{\lambda}_{\mathrm{thr}}$, that facilitates the

separation between the SS and NS eigenvalues, thus allowing for the determination of the numerical rank of $\hat{\mathbf{R}}_x$.

III. Covariance Matrix and Eigenvalue Analyses

We now consider a scenario in which some of the signals are weaker than the others. For such a scenario, we assume L_s strong signals and L_w weak signals such that the total number of signals is $L = L_s + L_w$. Let $\mathbf{R}_x$ denote the covariance matrices of the received data without weak signals (i.e., all L signals have equal signal power σ_s^2) and $\mathbf{R}_{wx}$ that with weak signals (i.e., L_w out of the L signals have a weaker power $\sigma_w^2 \leq \sigma_s^2$). Their difference is denoted as $\Delta\mathbf{R}$, i.e.,

$$\mathbf{R}_x = \mathbf{R}_{wx} + \Delta\mathbf{R}. \tag{10}$$

Because the trace of a covariance matrix is the summation of all the signal and noise powers, we have

$$\mathrm{Tr}(\mathbf{R}_x) = NL\sigma_s^2 + N\sigma_{\mathrm{n}}^2, \tag{11}$$

and

$$\mathrm{Tr}(\mathbf{R}_{wx}) = NL_s\sigma_s^2 + NL_w\sigma_w^2 + N\sigma_{\mathrm{n}}^2, \tag{12}$$

where σ_s^2 and σ_w^2 are respectively the powers of the strong and weak signals. Therefore, the difference between these traces is $\mathrm{Tr}(\mathbf{R}_x) - \mathrm{Tr}(\mathbf{R}_{wx}) = NL_w\Delta\sigma$, where $\Delta\sigma = \sigma_s^2 - \sigma_w^2$ denotes the power difference between the strong and weak signals.

The Weyl's theorem provides insights into the relationship between the eigenvalues of matrices $\mathbf{R}_x$ and $\mathbf{R}_{wx}$.

Weyl's theorem: [36] *Let* $\mathbf{A}$ *and* $\mathbf{B}$ *be two* $n \times n$ *Hermitian matrices. The eigenvalues of* $\mathbf{A}+\mathbf{B}$ *are related to those of* $\mathbf{A}$ *and* $\mathbf{B}$ *as*

$$\lambda_j(\mathbf{A}+\mathbf{B}) \leq \lambda_i(\mathbf{A}) + \lambda_{j-i+1}(\mathbf{B}) \;\; \textit{for} \;\; i \leq j, \tag{13}$$

and

$$\lambda_j(\mathbf{A}+\mathbf{B}) \geq \lambda_i(\mathbf{A}) + \lambda_{j-i+n}(\mathbf{B}) \;\; \textit{for} \;\; i \geq j. \tag{14}$$

For the underlying problem, we can replace $\mathbf{A}$ by $\mathbf{R}_{wx}$ and $\mathbf{B}$ by $\Delta\mathbf{R}$, where $\lambda_{L_w+1}(\Delta\mathbf{R}) = \cdots = \lambda_N(\Delta\mathbf{R}) = 0$. In the special case of a single weak signal ($L_w = 1$), we can obtain the following interlacing relationship from (10), (13), and (14):

$$\lambda_{i+1}(\mathbf{R}_x) \leq \lambda_i(\mathbf{R}_{wx}) \leq \lambda_i(\mathbf{R}_x) \tag{15}$$

for $1 \leq i \leq N-1$, which implies

$$\begin{aligned}\lambda_1(\mathbf{R}_x) \geq \lambda_1(\mathbf{R}_{wx}) \geq \lambda_2(\mathbf{R}_x) \geq \lambda_2(\mathbf{R}_{wx}) \\ \geq \cdots \geq \lambda_N(\mathbf{R}_x) \geq \lambda_N(\mathbf{R}_{wx}).\end{aligned} \tag{16}$$

IV. Effects of Sensor Locations and Signal Power on Smallest SS Eigenvalues

In this section, we examine the smallest SS eigenvalue of the covariance matrix for a non-integer array compared to its integer array counterpart and the effect of the weak signal power on the smallest SS eigenvalue. Two scenarios are considered to construct non-integer arrays as follows: (a) shifting one of the sensors in an integer array from its original position, say p_l, to a non-integer position $\tilde{p}_l$ between p_{l-1} and p_{l+1}, and (b) compressing the inter-element spacing of an integer array by a factor of $\alpha \leq 1$, rendering a ULA with its inter-element spacing generally smaller than half-wavelength. In both scenarios, we analyze the variation of the SS eigenvalues of the array covariance matrix with and without the presence of weak signals, with an emphasis on the numerical evaluation of the ratio between the largest and the smallest SS eigenvalues.

In the numerical evaluations, we consider an integer ULA with $N = 10$ sensors and $L = 9$ signals uniformly distributed in $[-60^\circ, 60^\circ]$. When considering the presence of weak signals, $L_s = 6$ strong and $L_w = 3$ weak signals are assumed. The six strong signals impinge from $-60^\circ, -45^\circ, -30^\circ, -15^\circ, 0^\circ$, and 15°, whereas the three weak signals arrive from $30^\circ, 45^\circ$, and 60°. The input signal-to-noise ratio (SNR) of the strong signals is set to 5 dB and that for the weak signals is -5 dB. In addition, 1,000 snapshots are used.

We first examine the ratio between the largest and the smallest SS eigenvalues of the covariance matrix when the fifth ULA sensor, originally placed at $p_5 = 4$ in the integer array, moves towards one of its two neighboring sensors, respectively located at $p_4 = 3$ and $p_6 = 5$. It is observed in Fig. 1(a) that, as the fifth sensor moves its position to $\tilde{p}_5$ away from its original position p_5 in either direction, the magnitude of the eigenvalue ratio increases, implying that reduction of the smallest SS eigenvalue. Eventually, as the fifth sensor moves very close to one of the adjacent sensor positions at $p_4 = 3$ and $p_6 = 5$, the smallest SS eigenvalue becomes very small, rendering a high value of the eigenvalue ratio. As a result, the contribution of the fifth sensor to the array DOFs tends to vanish. On the other hand, compared to the equal signal power case, the eigenvalue ratio in the presence of weak signals becomes higher because the smallest SS eigenvalue is smaller in this case.

In Fig. 1(b), it is observed that the eigenvalue ratio monotonically increases as the compression ratio α becomes smaller. That is, the smallest SS eigenvalue decreases as α takes a smaller value. Similar to the case depicted in Fig. 1(a), the eigenvalue ratio takes a higher value when weak signals are present.

Fig. 1(c) depicts the smallest SS eigenvalue $\hat{\lambda}_L$ with respect to the power of the weak signal as the location of the fifth sensor $\tilde{p}_5$ varies between 3.1 and 3.5. The value of $\hat{\lambda}_L$ varies monotonically with the sensor position as well as the power of the weak signal. On the other hand, for the different scenarios considered in this plot, the threshold obtained from the QR-factorization is nearly constant. As a result, the condition that the DOF contributed by the fifth sensor vanishes, i.e., the magnitude of $\hat{\lambda}_L$ goes below the threshold, is determined by both factors, namely, the position of the fifth sensor and the power of the weak signals. It is clear that the contribution of the fifth sensor is more pronounced when the power of the

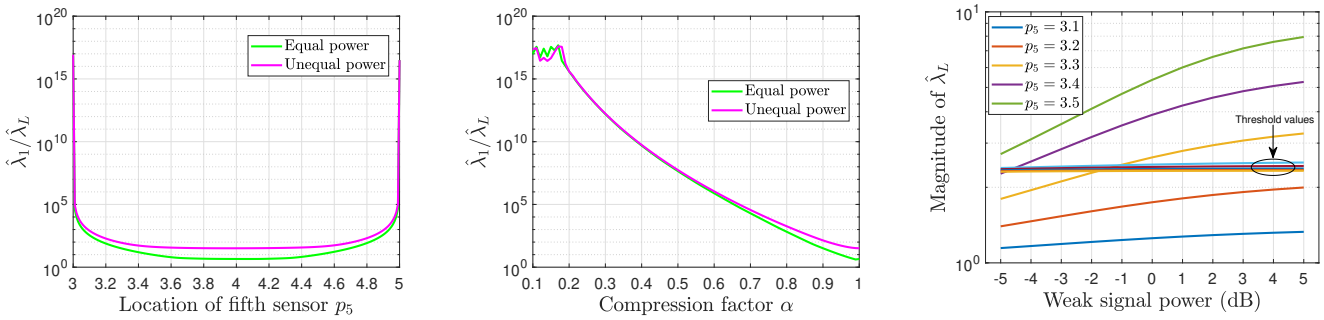

(a) Shifting sensor position $\tilde{p}_5$ (b) Compressing the ULA (c) $\hat{\lambda}_L$ vs. weak signal power

Fig. 1: Variation of the smallest SS eigenvalue with varying sensor location, compression factor, and signal power.

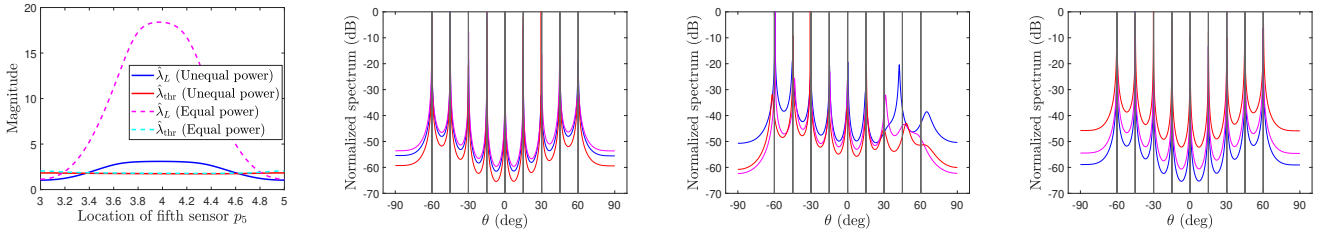

(a) $\hat{\lambda}_L$ and $\hat{\lambda}_{\text{thr}}$ with varying sensor location $\tilde{p}_5$ with and without weak signals

(b) All 9 signals are detected when 6 strong and 3 weak signals are present with $\tilde{p}_5 = 4.4$

(c) Not all 9 signals are detected when 6 strong and 3 weak signals are present with $\tilde{p}_5 = 4.7$

(d) All 9 signals are detected when all signals have equal power and $\tilde{p}_5 = 4.7$

Fig. 2: Eigenvalues and MUSIC spectra when the sensor position $\tilde{p}_5$ is shifted.

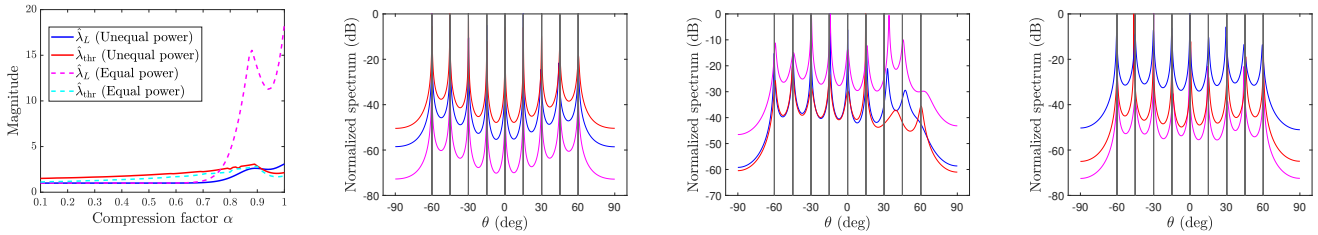

(a) $\hat{\lambda}_L$ and $\hat{\lambda}_{\text{thr}}$ with varying compression factor α with and without weak signals

(b) All 9 signals are detected when 6 strong and 3 weak signals are present with $\alpha = 0.95$

(c) Not all 9 signals are detected when 6 strong and 3 weak signals are present with $\alpha = 0.83$

(d) All 9 signals are detected when all signals have equal power and $\alpha = 0.83$

Fig. 3: Eigenvalues and MUSIC spectra when the inter-element spacing of the ULA is compressed.

weak signal is higher and when the sensor position is closer to the original integer position.

V. DOA Estimation Performance

To support our findings discussed in the previous sections, we evaluate the DOA estimation performance obtained from the MUSIC algorithm for the aforementioned two scenarios, namely, when the array sensors are shifted and when the inter-element spacing of the ULA is compressed. The effect of the presence of weak signals on the QR factorization threshold and the smallest SS eigenvalues is demonstrated and compared to the case when all signals have the same power. We consider a ULA consisting of $N = 10$ sensors with $L = 9$ uncorrelated signals uniformly distributed in $[-60°, 60°]$. The same signal parameters as those described in Section IV are used.

A. Moving a Sensor to an Off-Grid Position

For the first scenario, we consider that the fifth sensor, originally located at $p_5 = 4$, is shifted to a fractional location located between $p_5 = 3$ and $p_5 = 5$. Fig. 2(a) shows the estimated smallest SS eigenvalue $\hat{\lambda}_L$ and the QR factorization threshold $\hat{\lambda}_{\text{thr}} = ||\mathbf{R}_{22}||_2$ with respect to the location of the fifth sensor, $\tilde{p}_5$. It is observed that, in the presence of weak signals, the magnitude of $\hat{\lambda}_L$ is much smaller than that obtained form the scenario where all signals are of equal power. We also note that, for the unequal power scenario,

when $\tilde{p}_5 < 3.39$ or $\tilde{p}_5 > 4.62$, $\hat{\lambda}_L$ falls below the threshold, i.e., $\hat{\lambda}_L < \hat{\lambda}_{\rm thr}$. Accordingly, the numerical rank of $\hat{\mathbf{R}}_{xw}$, which represents the number of identifiable signals of the array, drops from 9 to 8. On the other hand, when all signals are assumed to have equal power, the magnitude of $\hat{\lambda}_L$ takes a much higher value. Correspondingly, the possible range of the off-grid sensor location without losing a DOF is much broader, ranging from $\tilde{p}_5 = 3.19$ to $\tilde{p}_5 = 4.80$. As a result, the DOF contributed by the moving sensor vanishes more easily in the presence of weak signals.

To confirm the validity of the claimed identifiability conditions, we show the MUSIC spectra of three independent trials in Figs. 2(b)–2(d). In Fig. 2(b), it is observed that, in the presence of weak signals with $\tilde{p}_5 = 4.5$, which is within the detectable threshold range between 3.39 and 4.62, all $L = 9$ signals are correctly detected. On the other hand, when we choose $\tilde{p}_5 = 4.7$, which is outside of the detectable range, the MUSIC spectra depicted in Fig. 2(c) show that some of the weak signals are not correctly detected. In contrast, when all the signals are assumed to be of the same strong power, the value of $\tilde{p}_5 = 4.7$ falls in the detectable threshold range between 3.19 and 4.80. In this case, it is observed in Fig. 2(d) that the array successfully resolves all signals.

B. Compressing the Inter-Element Spacing of the Entire ULA

Fig. 3(a) shows the estimated smallest SS eigenvalue $\hat{\lambda}_L$ and the QR factorization threshold $\hat{\lambda}_{\rm thr}$ with respect to the compression factor α for both scenarios respectively with equal and unequal signal powers. It is observed that, for the equal power case, the smallest SS eigenvalue $\hat{\lambda}_L$ is above the threshold $\lambda_{\rm thr}$ when $\alpha > 0.77$. On the other hand, when the three signals have a weak power, we require $\alpha = 0.91$ to keep $\hat{\lambda}_L$ to be above the threshold $\hat{\lambda}_{\rm thr}$. Such results are consistent with the observations made in Fig. 1(b) that the array is more sensitive to the sensor location in the presence of weak signals.

Fig. 3(b) shows the MUSIC spectra of the array in the presence of weak signals, where the compression factor is $\alpha = 0.95$. In this case, all the $L = 9$ signals are detected. As the compression factor is reduced to $\alpha = 0.83$, as shown in Fig. 3(c), the array fails to correctly identify the weak signals. In contrast, when all signals have equal power, $\alpha = 0.83$ still falls in the detectable region and, as a result, the MUSIC spectra shown in Fig. 3(d) indicate that all 9 signals are successfully resolved.

VI. Conclusion

In this paper, we investigated the signal identifiability of an array in the presence of mixed strong and weak signals when the sensor positions deviate from those located on a half-wavelength grid. Two scenarios are considered, namely, (1) when one sensor moves between its neighboring sensor positions and (2) when the array remains uniformly spaced but the inter-element spacing is compressed. We observed the conditions for these resulting non-integer array positions to maintain the number of original DOFs by examining the smallest SS eigenvalue in connection to changes in sensor positions and signal power. The rank-revealing QR factorization was applied to this analysis, and the signal identifiability was presented in terms of the numerical rank of the covariance matrix.

VII. References

[1] H. L. Van Trees, *Optimum Array Processing: Part IV of Detection, Estimation, and Modulation Theory*. Wiley, 2002.

[2] M. Skolnik, *Radar Handbook, 3rd Edition.* McGraw Hill, 2008.

[3] T. E. Tuncer and B. Friedlander (Eds.), *Classical and Modern Direction-of-Arrival Estimation*. Academic Press, 2009.

[4] P. Pal and P. P. Vaidyanathan, "Nested arrays: A novel approach to array processing with enhanced degrees of freedom," *IEEE Trans. Signal Process.*, vol. 58, no. 8, pp. 4167–4181, Aug. 2010.

[5] P. P. Vaidyanathan and P. Pal, "Sparse sensing with co-prime samplers and arrays," *IEEE Trans. Signal Process.*, vol. 59, no. 2, pp. 573–586, Feb. 2011.

[6] S. Qin, Y. D. Zhang, and M. G. Amin, "Generalized coprime array configurations for direction-of-arrival estimation," *IEEE Trans. Signal Process.*, vol. 63, no. 6, pp. 1377–1390, March 2015.

[7] A. Ahmed, Y. D. Zhang, and B. Himed, "Effective nested array design for fourth-order cumulant-based DOA estimation," in *Proc. IEEE Radar Conf.*, Seattle, WA, May 2017, pp. 998–1002.

[8] J. Liu, Y. Zhang, Y. Lu, S. Ren, and S. Cao, "Augmented nested arrays with enhanced DOF and reduced mutual coupling," *IEEE Trans. Signal Process.*, vol. 65, no. 21, pp. 5549–5563, Nov. 2017.

[9] Z. Zheng, W. Wang, Y. Kong and Y. D. Zhang, "MISC Array: A new sparse array design achieving increased degrees of freedom and reduced mutual coupling effect," *IEEE Trans. Signal Process.*, vol. 67, no. 7, pp. 1728–1741, April 2019.

[10] S. Sun and Y. D. Zhang, "4D automotive radar sensing for autonomous vehicles: A sparsity-oriented approach," *IEEE Sel. Topics Signal Process.*, vol. 15, no. 4, pp. 879–891, June 2021.

[11] A. Ahmed and Y. D. Zhang, "Generalized non-redundant sparse array designs," *IEEE Trans. Signal Process.*, vol. 69, pp. 4580–4594, Aug. 2021.

[12] W. Shi, Y. Li, and R. C. de Lamare. "Novel sparse array design based on the maximum inter-element spacing criterion," *IEEE Signal Process. Lett.*, vol. 29, pp. 1754–1758, July 2022.

[13] S. Wandale and K. Ichige, "Flexible extended nested arrays for DOA estimation: Degrees of freedom perspective," *Signal Process.*, vol. 201, no. 108710, pp. 1–10, Dec. 2022.

[14] Y. Lo, "A mathematical theory of antenna arrays with randomly spaced elements," *IEEE Trans. Antenna Propagat.*, vol. 12, no. 3, pp. 257–268, May 1964.

[15] B. Steinberg, "The peak sidelobe of the phased array having randomly located elements," *IEEE Trans. Antenna Propagat.*, vol. 20, no. 2, pp. 129–136, March 1972.

[16] P. Kulkarni and P. P. Vaidyanathan, "Non-integer arrays for array signal processing," *IEEE Trans. Signal Process.*, vol. 70, pp. 5457–5472, 2022.

[17] Y. I. Abramovich, N. K. Spencer and A. Y. Gorokhov, "DOA estimation for noninteger linear antenna arrays with more uncorrelated sources than sensors," *IEEE Trans. Signal Process.*, vol. 48, no. 4, pp. 943–955, April 2000.

[18] P. J. Bevelacqua and C. A. Balanis, "Optimizing antenna array geometry for interference suppression," *IEEE Trans. Antennas Propagat.*, vol. 55, no. 3, pp. 637–641, March 2007.

[19] S. M. Hosseini and M. Karimi, "Optimal design of nonredundant sparse arrays with noninteger distance between elements," *IEEE Sensors J.*, vol. 23, no. 17, pp. 20012–20019, Sept. 2023.

[20] P. Kulkarni and P. P. Vaidyanathan, "Rational arrays for DOA estimation," in *Proc. 2022 IEEE Int. Conf. Acoust., Speech Signal Process. (ICASSP)* , Singapore, 2022, pp. 5008–5012.

[21] Y. D. Zhang and M. G. Amin, "Multi-frequency rational sparse array for direction-of-arrival estimation," in *Proc. Int. Symp. Signals, Circuits and Systems*, Iași, Romania, July 2023, pp. 1–4.

[22] S. Qin, Y. D. Zhang, M. G. Amin, and B. Himed, "DOA estimation exploiting a uniform linear array with multiple co-prime frequencies," *Signal Process.*, vol. 130, pp. 37–46, Jan. 2017.

[23] A. Liu, X. Zhang, Q. Yang, and W. Deng, "Fast DOA estimation algorithms for sparse uniform linear array with multiple integer frequencies," *IEEE Access*, vol. 6, pp. 29952–29965, 2018.

[24] S. Zhang, A. Ahmed, Y. D. Zhang, and S. Sun, "Enhanced DOA estimation exploiting multi-frequency sparse array," *IEEE Trans. Signal Process.*, vol. 69, pp. 5935–5946, Oct. 2021.

[25] Y. D. Zhang and M. W. T. S. Chowdhury, "Frequency-switching sparse arrays," in *Proc. IEEE Sensor Array and Multich. Signal Process. (SAM) Workshop*, Corvallis, OR, July 2024.

[26] M. W. T. S. Chowdhury and Y. D. Zhang, "Unambiguous DOA estimation using multi-frequency rational sparse arrays," in *Proc. Asilomar Conf. Signals, Syst. Comput.*, Pacific Grove, CA, Oct. 2023, pp. 1324–1328.

[27] M. W. T. S. Chowdhury, Y. D. Zhang, W. Liu, and M. S. Greco, "Identifiability analysis of sensor arrays with sensors off half-wavelength grid," in *Proc. IEEE Int. Conf. Acoust., Speech, Signal Process. (ICASSP)*, Seoul, Korea, April 2024, pp. 8496–8500.

[28] V. T. Ermolaev and A. B. Gershman, "Fast algorithm for minimum-norm direction-of-arrival estimation," *IEEE Trans. Signal Process.*, vol. 42, no. 9, pp. 2389–2394, Sept. 1994.

[29] T. F. Chan and P. C. Hansen, "Some applications of the rank revealing QR factorization," *SIAM J. Scientific Stat. Comput.*, vol. 13, pp. 727–741, 1992.

[30] M. Gu and S. C. Eisenstat, "Efficient algorithms for computing a strong rank revealing QR factorization," *SIAM J. Scientific Comput.*, vol. 17, pp. 848–869, 1996.

[31] S. Ubaru, Y. Saad, and A. Seghouane, "Fast estimation of approximate matrix ranks using spectral densities," *Neural Comput.*, vol. 29, no. 5, pp. 1317–1351, May 2017.

[32] Y. P. Hong, and C.T. Pan, "Rank-revealing QR factorizations and the singular value decomposition," *Math. Comput.*, vol. 58, no. 197, 1992, pp. 213–232.

[33] J. A. Ball, I. Gohberg, L. Rodman, and T. Shalom, "On the eigenvalues of matrices with given upper triangular part," *Integral Equ. Oper. Theory*, vol. 13, pp. 488–497, 1990.

[34] W. H. Haemers, "Interlacing eigenvalues and graphs," *Linear Algebra App.*, vol. 226, pp. 593–616, 1995.

[35] X. Chen, and S. N. Zheng, "A unified proof of interlacing properties of eigenvalues of totally positive matrices," *Linear Algebra App.*, vol. 632, pp. 241–245, Jan. 2022.

[36] Y. Nakatsukasa, "Absolute and relative Weyl theorems for generalized eigenvalue problems," *Linear Algebra App.*, vol. 432, no. 1, 2010, pp. 242–248.